Mathematical and Computational Applications

MDPI

Article

Mathematical Modeling and Analysis of Ebola Virus Disease Dynamics: Implications for Intervention Strategies and Healthcare Resource Optimization

Ikram Ullah [1], Imtiaz Ahmad [1], Nigar Ali [1], Ihtisham Ul Haq [1], Mohammad Idrees [1], Mohammed Daher Albalwi [2] and Mehmet Yavuz [3,4,*]

[1] Department of Mathematics, University of Malakand, Chakdara 18000, Dir Lower, Khyber Pakhtunkhwa, Pakistan; ikramuom61@gmail.com (I.U.); iahmaad@hotmail.com (I.A.); nigaruom@gmail.com (N.A.); ihtisham0095@gmail.com (I.U.H.); mohammadidreesbjr8@gmail.com (M.I.)
[2] Yanbu Industrial College, The Royal Commission for Jubail and Yanbu, Yanbu 30436, Saudi Arabia; albalwim@rcjy.edu.sa
[3] Department of Mathematics and Computer Sciences, Faculty of Science, Necmettin Erbakan University, Konya 42090, Türkiye
[4] Centre for Environmental Mathematics, Faculty of Environment, Science and Economy, University of Exeter, Cornwall TR10 9FE, UK
* Correspondence: mehmetyavuz@erbakan.edu.tr

Abstract: This study implements a minded approach to studying Ebola virus disease (EVD) by dividing the infected population into aware and unaware groups and including a hospitalized compartment. This offers a more detailed understanding of illness distribution, potential analyses, and the influence of public knowledge. The findings might improve healthcare budget apportionment, public health policy, and contest Ebola and related infections. In this study, we fully observe the new model $SEIHR$ that we have constructed. We start by outlining the essential concepts of the model and confirming its mathematical reliability. Next, we calculate the fundamental reproductive number (R_0), which is critical for appreciating how the infection spreads and how effective treatments might be. We also study stability analysis, which looks at when the disease may decline or become chronic. Furthermore, we exhibit the occurrence of bifurcation in the EVD Epidemic Model and perform a sensitivity analysis of (R_0). The main findings of this study show that for $R_0 < 1$, the disease-free equilibrium, is globally stable, meaning the disease will die out, whereas for $R_0 > 1$, the endemic equilibrium is stable, meaning the disease persists. Additionally, the sensitivity analysis reveals that the most influential parameters in controlling R_0 are the transmission rate and the recovery rate, which could guide effective intervention strategies. Finally, we use numerical simulations so that out outcomes are more significant.

Keywords: $SEIHR$ mathematical model; Ebola virus; stability analysis; bifurcation; numerical simulation

check for updates

Citation: Ullah, I.; Ahmad, I.; Ali, N.; Haq, I.U.; Idrees, M.; Albalwi, M.D.; Yavuz, M. Mathematical Modeling and Analysis of Ebola Virus Disease Dynamics: Implications for Intervention Strategies and Healthcare Resource Optimization. *Math. Comput. Appl.* **2024**, *29*, 94. https://doi.org/10.3390/mca29050094

Academic Editor: Alexandre Souto Martinez

Received: 1 August 2024
Revised: 19 September 2024
Accepted: 9 October 2024
Published: 12 October 2024

Copyright: © 2024 by the authors. Licensee MDPI, Basel, Switzerland. This article is an open access article distributed under the terms and conditions of the Creative Commons Attribution (CC BY) license (https://creativecommons.org/licenses/by/4.0/).

1. Introduction

Ebola virus disease (EVD) is caused by a virus that most likely originated in flying foxes, often known as fruit bats. These bats can transfer and spread the virus to humans [1]. The first cases of Ebola were noted in 1976, following severe fever epidemics in Central Africa. Interacting with animals such as porcupines, monkeys, apes, and fruit bats, which are natural hosts of the Ebola virus, increases the risk of transmission. These animals may transfer the virus without symptoms, serving as reservoirs in their natural environments. When people come into contact with them, particularly in areas where Ebola is prevalent, they risk contracting the virus. Contact with biological fluids such as blood, saliva, and urine, as well as activities such as hunting, can spread the infection. Understanding these transmission routes is essential for preventing outbreaks and protecting public health. Educating people about the risks of handling these animals and encouraging safe practices

in doing so is important for containing the spread of Ebola and reducing its impact on both human and animal communities. Healthcare workers and aid staff can also contract the virus while treating patients in healthcare facilities [2,3]. Health authorities have launched workshops and educational programs for doctors in Pakistan [4], acknowledging the epidemic threat of Ebola.

Various fields have used mathematical modeling to observe different aspects of diseases and their dynamics [5–15]. These models can encompass a wide range of medical resources or focus on specific elements such as hospital beds and laboratory equipment. For example, Zhou and Fan [5] examined human behavior in the presence of scarce medical resources using an SIR model, which takes into account susceptibility, infection, and recovery. Their results revealed that individuals tend to adopt more protective measures when faced with limited treatment and prevention options for highly deadly diseases.

The Ebola virus disease has been widely studied using mathematical models that consider limited resources. In a study by Nouvellet et al. [6], an $SEIR$ model was developed, incorporating delays between different stages of the disease, to highlight the importance of rapid diagnostic tests for Ebola. Similarly, Leward et al. [7] examined pharmacological interventions to control EVD and arrived at similar conclusions. In 2020, Rafiq et al. [14] analyzed a model that classified the population into four groups: susceptible individuals ($S(t)$), exposed individuals ($E(t)$), infected individuals ($I(t)$), and individuals who have recovered ($R(t)$). Their focus was on evaluating the stability of the different equilibrium points of the model [14]. Previous studies have explored various strategies for controlling Ebola, emphasizing the importance of proactive measures in managing outbreaks [10,11,16].

This study introduces key innovations compared to prior work. Specifically, we divide the infected population into two distinct groups: "aware" and "unaware" individuals, based on their knowledge of the disease. Furthermore, we include a hospitalized compartment to account for the role of healthcare facilities in controlling the outbreak. Unlike previous models, which primarily focused on general population compartments, our model provides a more granular analysis of public health interventions. This approach allows us to assess the impact of public awareness campaigns and hospital capacity on disease dynamics, making our contribution unique in highlighting the importance of behavioral and structural interventions in managing EVD outbreaks.

The rest of the paper is organized as follows: Section 2 outlines the model formulation. Then, Section 3 discusses how the model is well-posed, with subsections focusing on specific aspects like Invariant Regions and the Positivity of Solutions. Section 4 discusses Steady States, with subsections on the Disease-Free Equilibrium Point (DFE) and the Endemic Equilibrium Point (EE). The Basic Reproductive Number (R_0) is computed in Section 5. Sections 6 and 7 analyze the stability of the model, both locally and globally, considering equilibrium points. Section 8 discusses the existence of Bifurcation within the model. Sensitivity Analysis of R_0 is performed in Section 9, followed by Numerical Simulations in Section 10. Finally, Section 11 concludes the paper.

2. Model Formulation

In order to understand how Ebola spreads between humans and animals, we have modified $SEIHR$ model for Ebola transmission. This model categorizes the total population into six groups over time. $S(t)$ represents susceptible individuals who are at risk of contracting Ebola, $E(t)$ denotes the exposed class who have been in contact with the Ebola virus but are not yet showing symptoms, $I_u(t)$ signifies infected individuals who are unaware of their infection at the current time, $I_a(t)$ indicates infected individuals who are aware of their infection at the current time, $H(t)$ represents hospitalized individuals who require medical care, and $R(t)$ denotes recovered individuals who are no longer infectious. The flowchart and parameter descriptions are given in Figure 1 and Table 1, respectively. Through this model, we track the movement of individuals between these categories to understand the dynamics of Ebola transmission among humans and animals. In this study, the following model is considered:

$$\begin{cases} \frac{dS}{dt} = \Lambda - \mu S - (\alpha_1 + \eta_1 + \sigma_1)SE - (\sigma_2 + \eta_2)SI_u - (\sigma_3 + \eta_3)SI_a, \\ \frac{dE}{dt} = (\alpha_1 + \eta_1 + \sigma_1)SE - \alpha_2 I_u E - \alpha_3 I_a E - (\mu + \delta_1)E, \\ \frac{dI_u}{dt} = (\sigma_2 + \eta_2)SI_u + \alpha_2 I_u E - \alpha_4 H I_u - (\mu + \delta_2 + \alpha_6)I_u, \\ \frac{dI_a}{dt} = (\sigma_3 + \eta_3)SI_a + \alpha_3 I_a E - \alpha_5 H I_a - (\mu + \delta_3 + \alpha_7)I_a, \\ \frac{dH}{dt} = \alpha_4 H I_a + \alpha_5 H I_u - (\mu + \delta_4 + \alpha_8)H, \\ \frac{dR}{dt} = \alpha_6 I_u + \alpha_7 I_a + \alpha_8 H - \mu R. \end{cases} \tag{1}$$

with initial conditions: $S(0) > 0$, and $(E(0),\ I_u(0),\ I_a(0),\ H(0),\ R(0)) \geq 0$. The mathematical model is illustrated in the flowchart in Figure 1, and the description of the parameters is provided in Table 1.

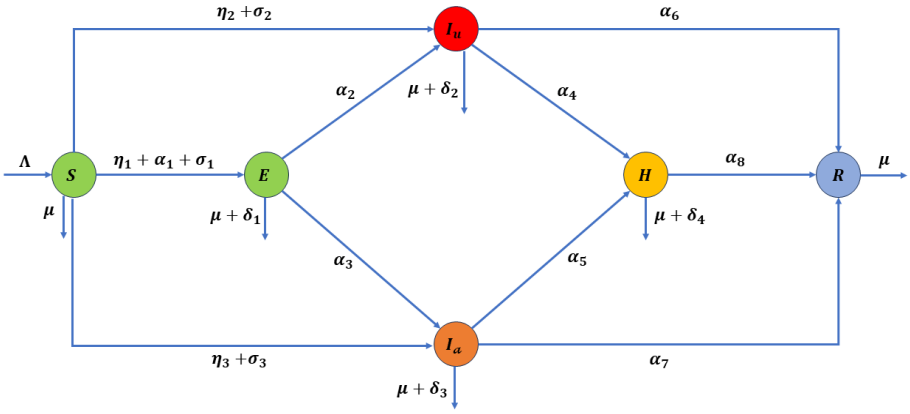


Figure 1. Flowchart of the Ebola virus.

Table 1. Parameter descriptions.

Parameter	Description
Λ	New recruitment rate
μ	Natural mortality rate
δ_1	Death rate due to disease for exposed individuals
δ_2	Mortality rate due to disease for unaware individuals
δ_3	Mortality rate due to disease for aware individuals
δ_4	Mortality rate due to disease for hospitalized individuals
α_1	Rate of infection from susceptible to exposed humans
α_2	Transmission rate from exposed to unaware persons
α_3	Rate of transmission from exposed to aware peoples
α_4	Transmission rate from individuals in the unaware state to those in the hospitalized state
α_5	Transmission rate from individuals in the aware state to those in the hospitalized state
α_6	Transmission rate from individuals in the unaware state to those in the recovered state
α_7	Transmission rate from individuals in the aware state to those in the recovered state
α_8	Transmission rate from individuals in the hospitalized state to those in the recovered state
η_1	Infection rate from wild animals to individuals in the exposed state
η_2	Infection rate from wildlife to individuals in the unaware state
η_3	Infection rate from wildlife to individuals in the aware state
σ_1	Infection rate from domestic animals to individuals in the exposed state
σ_2	Infection rate from domestic animals to individuals in the unaware state
σ_3	Infection rate from domestic animals to individuals in the aware state

3. Well-Posedness of the Proposed Model

3.1. Invariant Region

Theorem 1. *Within the region* $\tau = \{(S,\ E,\ I_u,\ I_a,\ H,\ R) \in \mathbb{R}^6_+ : S > 0,\ (E,\ I_u,\ I_a,\ H,\ R) \geq 0,\ N \leq \frac{\Lambda}{\mu}\}$, *the system described by Equation* (1) *exhibits the existence and uniqueness of a solution given specific initial conditions. This region* τ *remains both attracting and positively invariant*

concerning the system's dynamics. The proof of its existence and uniqueness can be established using Picard's existence theorem.

Proof. The functions on the right-hand side of (1) are Lipschitz continuous, and they play a crucial role in Picard's existence theorem, which determines when solutions to the system are possible. This means that the system described by (1) has solutions that are both positive and bounded within a certain region τ. Now, let us talk about the total population, denoted by N and is given by

$$N = S + E + I_u + I_a + H + R. \tag{2}$$

By differentiating Equation (2) with respect to time and then putting the values from (1), we obtain

$$\frac{dN}{dt} + \mu N \leq \Lambda. \tag{3}$$

Solving (3) through the application of an integrating factor and incorporating the initial condition $N(0) = N_0$, we obtain

$$N \leq N_0 e^{-\mu t} + \frac{\Lambda}{\mu}(1 - e^{-\mu t}). \tag{4}$$

In (4), as t approaches infinity, N tends to $\frac{\Lambda}{\mu}$. Consequently, we observe that in system (1), the entire set of feasible solutions converges to the enclosed region τ. Thus, the closed region τ remains positively invariant at all times t, affirming the biological significance and mathematical coherence of model (1) within τ. □

3.2. Positivity of the Solutions

Our model aims to ensure biological realism. We aim to show that every path starting from the non-negative region $\mathbb{R}^6_+$ will ultimately converge to and stay within the feasible area τ. To prove this, we will establish that the set τ is positively invariant and is the system's global attractor [17].

Theorem 2. *Consider thagt the initial conditions of* (1) *are nonnegative, then the solutions for the different groups* $S,\ E,\ I_u,\ I_a,\ H$ *and* R *of system* (1) *remain nonnegative* $\forall\ t > 0$.

Proof. Take into consideration, $t' = \sup\{t > 0; S > 0, \text{and } (E,\ I_u,\ I_a,\ H,\ R) \geq 0\}$.

In that case, $t' > 0$, because $S(0) > 0$, also take

$$\frac{dS}{dt} = \Lambda - S[\mu + (\sigma_1 + \eta_1 + \alpha_1)E + (\sigma_2 + \eta_2)I_u + (\sigma_3 + \eta_3)I_a]. \tag{5}$$

Let $g(t) = (\sigma_1 + \eta_1 + \alpha_1)E + (\sigma_2 + \eta_2)I_u + (\sigma_3 + \eta_3)I_a$, then (5) becomes

$$\frac{dS}{dt} + (\mu + g(t))S = \Lambda. \tag{6}$$

After solving (6) and using $S(0) = S_0$, yields

$$S(t') = S_0 e^{(-\mu t' - \int_0^{t'} g(t)dt)} + \Lambda e^{(-\mu t' - \int_0^{t'} f(t)dt)} \int_0^{t'} e^{(\mu y + \int_0^y g(x)dx)} dy. \tag{7}$$

As $S_0 > 0$, $\Lambda > 0$ also $e^{(-\mu t' - \int_0^{t'} g(t)dt)}$, $e^{(-\mu t' - \int_0^{t'} f(t)dt)}$, and $\int_0^{t'} e^{(\mu y + \int_0^y g(x)dx)} dy$ are positive. Therefore, $S(t) > 0$.

From model (1), Equation (2) can be written as

$$\frac{dE}{dt} \geq -E(\alpha_2 I_u + \alpha_3 I_a) - (\mu + \delta_1)E. \tag{8}$$

Let $g_1(t) = \alpha_2 I_a + \alpha_3 I_u$. By solving (8) and using $E(0) = E_0$, we obtain

$$E \geq E_0 e^{(\mu + \mu_1)t} e^{\int -(g_1(t))dt}. \tag{9}$$

In (9) $E_0 \geq 0$, $e^{\int -(g_1(t))dt} > 0$ and $e^{(\mu+\mu_1)t} > 0$. and Therefore $E \geq 0$.

A similar procedure can be extended to the rest of the equations in model (1). This analysis shows that all the state variables we are tracking stay non-negative for any $t \geq 0$. This is important because it means our model's solutions always remain positive, which is crucial for its accuracy. □

4. Equilibrium Points

In disease modeling, steady states refer to situations where the number of people in each group remains constant over time. This happens when the rates at which people move between groups are balanced. It means the number of infected individuals remains stable over time for a specific value of R_0, no matter how many people were initially infected. Here, we discuss two types of steady states (disease-free equilibrium and endemic equilibrium).

4.1. Disease-Free Equilibrium Point (DFE)

To determine the DFE P_0 of System (1), each equation on the right-hand side of system (1) is set to zero. After simplifying and arranging the expressions, we obtain $P_0 = (S_0,\ E_0,\ I_{u_0},\ I_{a_0},\ H_0,\ R_0) = (\frac{\Lambda}{\mu},\ 0,\ 0,\ 0,\ 0,\ 0)$.

4.2. Endemic Equilibrium Point (EE)

Similarly, to determine the EE point $P_1 = (S_1,\ E_1,\ I_{u_1},\ I_{a_1},\ H_1,\ R_1)$ of System (1), each equation on the right-hand side of system (1) is set as zero. Simplifying and arranging formulas for the endemic point P_1 yields the following result:

$$S_1 = \frac{\Lambda(\alpha_4\alpha_3 - \alpha_5\alpha_2)}{\alpha_4(\mu\alpha_3 + b_1b_6 - b_3b_4) + \alpha_5(b_4b_2 - b_1b_5 - \mu\alpha_2) + b_7(\alpha_3b_2 - \alpha_2b_3)},$$

$$E_1 = \frac{\begin{array}{l}\alpha_4^2(\alpha_3(\mu b_6 - \Lambda b_3) + b_1b_6^2 - b_3b_4b_6) + \alpha_4(\alpha_5(\alpha_2(\Lambda b_3 - \mu b_6) + \alpha_3(\Lambda b_2 - \mu b_5) + b_5(b_3b_4 - 2b_1b_6) + b_2b_4b_6) \\ + b_6b_7(\alpha_3b_2 - \alpha_2b_3)) + \alpha_5(\alpha_5(\alpha_2(\mu b_5 - \Lambda b_2) + b_1b_5^2 - b_2b_4b_5) - b_5b_7(\alpha_3b_2 - \alpha_2b_3))\end{array}}{(\alpha_4(\mu\alpha_3 + b_1b_6 - b_3b_4) + \alpha_5(b_4b_2 - b_1b_5 - \mu\alpha_2) + b_7(\alpha_3b_2 - \alpha_2b_3))(\alpha_3\alpha_4 - \alpha_2\alpha_5)},$$

$$I_{u_1} = \frac{\begin{array}{l}\alpha_5^2(b_4b_2^2 - b_4(b_5b_1 + \mu\alpha_2) + \alpha_2\Lambda b_1) + \alpha_5(\alpha_3(\alpha_4(\mu b_4 - \Lambda b_1) - b_7(\mu\alpha_2 + b_5b_1) - 2b_4b_2) \\ + b_4(\alpha_4(b_6b_1 - b_4b_3 - \alpha_2b_7b_3)) + \alpha_3b_7(\alpha_3(\mu\alpha_4 + b_7b_2) + \alpha_4(b_6b_1 - b_4b_3) - \alpha_2b_7b_3)\end{array}}{(\alpha_5(b_4b_2 - b_5b_1 - \mu\alpha_2) + \alpha_3(\mu\alpha_4 + b_7b_2) + \alpha_4(b_6b_1 - b_4b_3) - \alpha_2b_7b_3)(\alpha_3\alpha_4 - \alpha_2\alpha_5)},$$

$$I_{a_1} = \frac{\begin{array}{l}\alpha_4^2(\alpha_3(\Lambda b_1 - \mu b_4) - b_4b_1b_6 + b_3b_4^2) + \alpha_4(\alpha_2(\alpha_5(\mu b_4 - \Lambda b_1) - b_7(\mu\alpha_3 + b_6b_1 - 2b_3b_4)) \\ + b_4(\alpha_5(b_5b_1 - b_2b_4)) - \alpha_3b_2b_7) + \alpha_2b_7(\alpha_2(\mu\alpha_5 + b_7b_3) + \alpha_5(b_5b_1 - b_2b_4) - \alpha_3b_2b_7)\end{array}}{(\alpha_4(\mu b_3 + b_6b_1 - b_4b_3) - \alpha_2(\mu\alpha_5 + b_7b_3) + \alpha_5(b_4b_2 - b_5b_1) + \alpha_3b_2b_7)(\alpha_3\alpha_4 - \alpha_2\alpha_5)},$$

$$H_1 = \frac{\begin{array}{l}\alpha_2^2(\alpha_5(\Lambda b_3 - \mu b_6) - b_3b_6b_7) + \alpha_2(\alpha_3(\alpha_4(\mu b_6 - \Lambda b_3) + \alpha_5(\mu b_5 - \Lambda b_2) + b_7(b_2b_6 + b_3b_5)) + b_6(\alpha_4(b_1b_6 - b_3b_4) \\ - \alpha_5(b_1b_5 - b_2b_4))) - \alpha_3(\alpha_3(\alpha_4(\mu b_5 - \Lambda b_2) + b_2b_5b_7) + b_5(\alpha_4(b_1b_6 - b_3b_4) - \alpha_5(b_1b_5 - b_2b_4)))\end{array}}{(\alpha_2(-\mu\alpha_5 - b_3b_7) + \alpha_3(\mu\alpha_4 + b_2b_7) + \alpha_4(b_1b_6 - b_3b_4) - \alpha_5(b_1b_5 - b_2b_4))(\alpha_3\alpha_4 - \alpha_2\alpha_5)},$$

$$R_1 = \frac{\begin{array}{l}\alpha_2^2(\alpha_5(\mu\alpha_7b_7 + \alpha_8(\Lambda b_3 - \mu b_6)) + b_3b_7(\alpha_7b_7 - \alpha_8b_6)) + \alpha_4(\alpha_3(\alpha_4(-\mu\alpha_7b_7 - \alpha_8(\Lambda b_3 - \mu b_6)) + \alpha_5(\mu\alpha_6b_7 \\ - \alpha_8(\Lambda b_2 - \mu b_5)) - b_7(b_7(\alpha_6b_3 + \alpha_7b_2) - \alpha_8(b_2b_6 + b_3b_5))) + \alpha_5(-\alpha_7(\Lambda b_1 - \mu b_4)) + b_4(2\alpha_7b_3b_7 - \alpha_8b_3b_6) \\ - b_1b_6(\alpha_7b_7 - \alpha_8b_6)) + \alpha_5(\alpha_6(\Lambda b_1 - \mu b_4)\alpha_5 + b_4(b_7(-\alpha_6b_3 - \alpha_7b_2) + \alpha_8\alpha_2b_6) + b_1b_5(\alpha_7b_7 - \alpha_8b_6))\alpha_2 \\ + \alpha_3^2(\alpha_4(\mu\alpha_6b_7 + \alpha_8(\Lambda b_2 - \mu b_5)) + b_2b_7(\alpha_6b_7 - \alpha_8b_5)) + \alpha_3(\alpha_7(\Lambda b_1 - \mu b_4)\alpha_4^2 + \alpha_4(-\alpha_6(\Lambda b_1 - \mu b_4)\alpha_5 \\ + b_4(b_7(-\alpha_6b_3 - \alpha_7b_2) + \alpha_8b_3b_5) + b_1b_6(\alpha_6b_7 - \alpha_8b_5)) - \alpha_5(b_4(-2\alpha_6b_2b_7 + \alpha_8b_2b_5) + b_1b_5(\alpha_6b_7 - \alpha_8b_5)))\end{array}}{\begin{array}{l}- (\alpha_4\alpha_7 - \alpha_5\alpha_6)\alpha_4(\alpha_4(b_1b_6 - b_3b_4) - \alpha_5(b_1b_5 - b_2b_4)) \\ (\alpha_2(-\mu\alpha_5 - b_3b_7) + \alpha_3(\mu\alpha_4 + b_2b_7) + \alpha_4(b_1b_6 - b_3b_4) - \alpha_5(b_1b_5 - b_2b_4))\mu(\alpha_3\alpha_4 - \alpha_2\alpha_5)\end{array}},$$

where $b_1 = (\eta_1 + \alpha_1 + \sigma_1)$, $b_2 = (\eta_2 + \sigma_2)$, $b_3 = (\eta_3 + \sigma_3)$, $b_4 = (\mu + \delta_1)$, $b_5 = (\mu + \delta_2 + \alpha_6)$, $b_6 = (\mu + \delta_3 + \alpha_7)$, and $b_7 = (\mu + \delta_4 + \alpha_8)$.

5. Basic Reproduction Number (R_0)

To find the basic reproduction number R_0 for model (1), the next-generation matrix method is employed. From model (1), attention is directed towards the infected classes, following procedures outlined in various papers such as [18]. Matrices F and V are as follows.

$$F = \begin{bmatrix} (\eta_1 + \alpha_1 + \sigma_1)SE - \alpha_2 I_u E - \alpha_3 I_a E \\ (\eta_2 + \sigma_2)SI_u + \alpha_2 I_u E - \alpha_3 H I_u \\ (\eta_3 + \sigma_3)SI_a + \alpha_3 I_a E - \alpha_5 H I_a \\ \alpha_4 H I_u + \alpha_5 H I_a \end{bmatrix}, \quad V = \begin{bmatrix} (\mu + \delta_1)E \\ (\mu + \delta_2 + \alpha_6)I_u \\ (\mu + \delta_3 + \alpha_7)I_a \\ (\mu + \delta_4 + \alpha_8)H \end{bmatrix}.$$

The Jacobian matrices for F and V at the disease-free equilibrium point are presented as F^* and V^* are given below;

$$F^* = \begin{bmatrix} \frac{\Lambda}{\mu}(\eta_1 + \sigma_1 + \alpha_1) & 0 & 0 & 0 \\ 0 & \frac{\Lambda}{\mu}(\eta_2 + \sigma_2) & 0 & 0 \\ 0 & 0 & \frac{\Lambda}{\mu}(\eta_3 + \sigma_3) & 0 \\ 0 & 0 & 0 & 0 \end{bmatrix}, \quad V^* = \begin{bmatrix} (\mu + \delta_1) & 0 & 0 & 0 \\ 0 & (\mu + \delta_2 + \alpha_6) & 0 & 0 \\ 0 & 0 & (\mu + \delta_3 + \alpha_7) & 0 \\ 0 & 0 & 0 & (\mu + \delta_4 + \alpha_8) \end{bmatrix}.$$

Thus, the next-generation matrix is given by

$$F^* \cdot V^{*^{-1}} = \begin{bmatrix} \frac{\Lambda(\eta_1 + \alpha_1 + \sigma_1)}{\mu(\mu + \delta_1)} & 0 & 0 & 0 \\ 0 & \frac{\Lambda(\eta_2 + \sigma_2)}{\mu(\mu + \delta_2 + \alpha_6)} & 0 & 0 \\ 0 & 0 & \frac{\Lambda(\eta_3 + \sigma_3)}{\mu(\mu + \delta_3 + \alpha_7)} & 0 \\ 0 & 0 & 0 & 0 \end{bmatrix}.$$

This matrix is diagonal, and thus its eigenvalues are as follows:

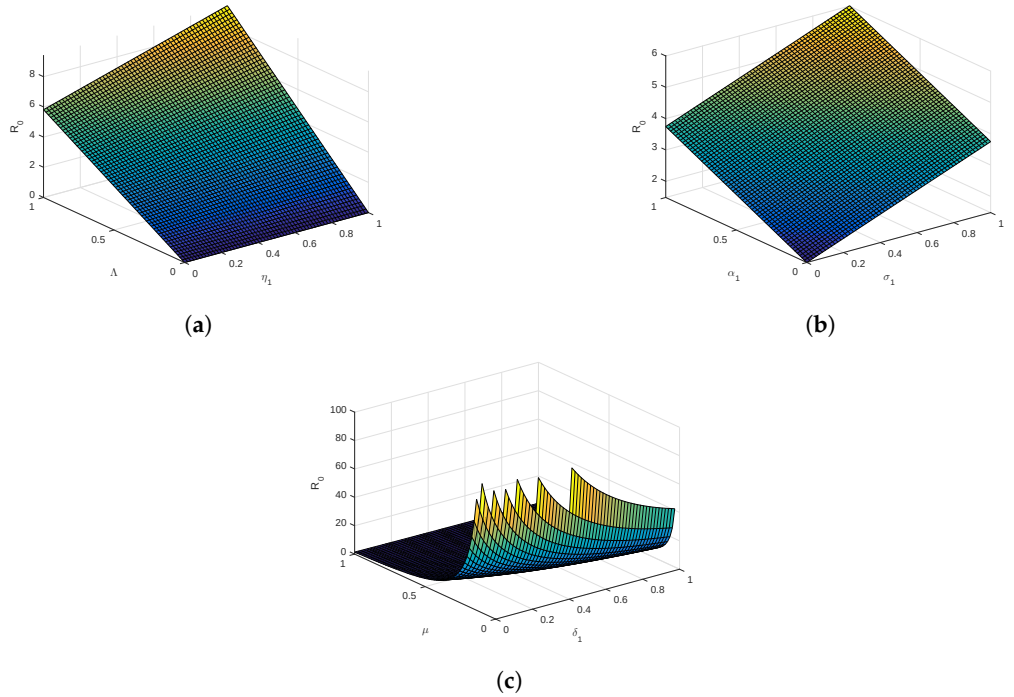
$$\lambda_1 = \frac{\Lambda(\eta_1 + \alpha_1 + \sigma_1)}{\mu(\mu + \delta_1)}, \quad \lambda_2 = \frac{\Lambda(\eta_2 + \sigma_2)}{\mu(\mu + \delta_2 + \alpha_6)}, \quad \lambda_3 = \frac{\Lambda(\eta_3 + \sigma_3)}{\mu(\mu + \delta_3 + \alpha_7)}, \quad \lambda_4 = 0.$$

The basic reproduction number, designated as R_0, and derived as the dominant eigenvalue of $F^* \cdot V^{*^{-1}}$. On completing the necessary computation, it is found that $R_0 = \max\{\lambda_1, \lambda_2, \lambda_3, \lambda_4\} = \lambda_1$, where λ_i, $i = 1, 2, 3, 4$ are eigenvalues derived from the calculation of the resulting matrix. Therefore,

$$R_0 = \frac{\Lambda(\eta_1 + \alpha_1 + \sigma_1)}{\mu(\mu + \delta_1)}. \tag{10}$$

Graphical representations are currently illustrating how parameters influence the basic reproductive number R_0.

Figure 2a,b demonstrate that R_0 is directly proportional to Λ, η_1, α_1, and σ_1. In Figure 2c, it is depicted that R_0 varies inversely with μ and δ_1.



(**a**) (**b**)

(**c**)

Figure 2. (**a**) The effect of Λ, η_1 on R_0. (**b**) The influence of α_1, σ_1 on R_0. (**c**) The effect of μ and δ_1 on R_0.

6. Local Stability Analysis of the Disease-Free Equilibrium (DFE) Point

This section entails conducting a local stability analysis of the DFE point P_0 for the model (1). We follow procedures outlined by various researchers [19,20] at $P_0 = (\frac{\Lambda}{\mu}, 0, 0, 0, 0, 0)$, with some particular initial population values of each class.

Theorem 3. *The model* (1) *is locally asymptotically stable at* P_0*, within* τ*, when* $R_0 < 1$*, and unstable if* $R_0 > 1$*.*

Proof. The Jacobian for system (1) at P_0 is below:

$$J(P_0) = \begin{pmatrix} -\mu & -\frac{\Lambda}{\mu}b_1 & -\frac{\Lambda}{\mu}b_2 & -\frac{\Lambda}{\mu}b_3 & 0 & 0 \\ 0 & \frac{\Lambda}{\mu}b_1 - b_4 & 0 & 0 & 0 & 0 \\ 0 & 0 & \frac{\Lambda}{\mu}b_2 - b_5 & 0 & 0 & 0 \\ 0 & 0 & 0 & \frac{\Lambda}{\mu}b_3 - b_6 & 0 & 0 \\ 0 & 0 & 0 & 0 & -b_7 & 0 \\ 0 & 0 & \alpha_6 & \alpha_7 & \alpha_8 & -\mu \end{pmatrix}.$$

where $b_1 = (\eta_1 + \alpha_1 + \sigma_1)$, $b_2 = (\eta_2 + \sigma_2)$, $b_3 = (\eta_3 + \sigma_3)$, $b_4 = (\mu + \delta_1)$, $b_5 = (\mu + \delta_2 + \alpha_6)$, $b_6 = (\mu + \delta_3 + \alpha_7)$, and $b_7 = (\mu + \delta_4 + \alpha_8)$.

From the above matrix, the eigenvalues are:

$$\lambda_1 = -\mu,\ \lambda_2 = -\mu,\ \lambda_3 = -(\mu + \delta_4 + \alpha_8),\ \lambda_4 = \frac{\Lambda}{\mu}(\eta_3 + \sigma_3) - (\mu + \delta_3 + \alpha_7),\ \lambda_5 = \frac{\Lambda}{\mu}(\eta_2 + \sigma_2) - (\mu + \delta_2 + \alpha_6),$$

$$\lambda_6 = (\mu + \delta_1)(R_0 - 1).$$

Here, $\lambda_1 = -\mu$, $\lambda_2 = -\mu$, because $\mu > 0$, $\lambda_3 = -(\mu + \delta_4 + \alpha_8) < 0$ as $(\mu + \delta_4 + \alpha_8) > 0$, $\lambda_4 = \frac{\Lambda}{\mu}(\eta_3 + \sigma_3) - (\mu + \delta_3 + \alpha_7) < 0$ if and only if $\frac{\Lambda}{\mu}(\eta_3 + \sigma_3) < (\mu + \delta_3 + \alpha_7)$, $\lambda_5 = \frac{\Lambda}{\mu}(\eta_2 + \sigma_2) - (\mu + \delta_2 + \alpha_6) < 0 \Leftrightarrow \frac{\Lambda}{\mu}(\eta_2 + \sigma_2) < (\mu + \delta_2 + \alpha_6)$, and finally, if $R_0 < 1$,

then all eigenvalues are less than 0, implying that $P_0 = (\frac{\Lambda}{\mu}, 0, 0, 0, 0, 0)$ is LAS, otherwise unstable. □

7. Global Stability Analysis

This portion entails conducting global stability of system (1). For this, we use the Lyapunov function method to establish global asymptotic stability (GAS) at both equilibrium points, following the approach outlined in [21,22].

7.1. Global Stability at DFE Point

Here, the main goal is to construct the Lyapunov function, a specialized mathematical formula that ensures system stability and facilitates reaching the desired state even when conditions change.

Theorem 4. *The disease-free equilibrium point P_0 of the EVD system (1) is globally asymptotically stable in τ when $R_0 < 1$.*

Proof. Demonstrating the global stability of model (1) at P_0, we consider $V : \tau \to \mathbb{R}$ [20] as a Lyapunov function:

$$V = S - S_0(\ln S) + E + I_u + I_a + H. \tag{11}$$

By differentiating (11) with respect to t and substituting the values from (1) into (11), we obtain:

$$\begin{aligned} \frac{dV}{dt} &= -\frac{\mu}{S}(S - S_0)^2 - (\mu + \delta_4 + \alpha_8)H + [(\mu + \delta_1)(R_0 - 1)]E \\ &+ [\frac{\Lambda}{\mu}(\eta_2 + \sigma_2) - (\mu + \delta_3 + \alpha_7)]I_u + [\frac{\Lambda}{\mu}(\eta_3 + \sigma_3) - (\mu + \delta_2 + \alpha_6)]I_a. \end{aligned} \tag{12}$$

As $\frac{\Lambda}{\mu}(\eta_2 + \sigma_2) < (\mu + \delta_3 + \alpha_7)$ and $\frac{\Lambda}{\mu}(\eta_2 + \sigma_2) < (\mu + \delta_2 + \alpha_6)$ from Theorem 3, $\frac{dV}{dt} \leq 0$ for $R_0 < 1$. Definitely, $\frac{dV}{dt} = 0$ only at $(S, E, I_u, I_a, H) = (S_0, 0, 0, 0, 0)$, and $\frac{dV}{dt} < 0$ otherwise. This shows $\frac{dV}{dt}$ is negative semi-definite around $P_0 = (S_0, 0, 0, 0, 0, 0)$, approving V as a Lyapunov function in τ. The point P_0 is the largest invariant subset where $\frac{dV}{dt} = 0$.

Anywhere a solution trajectory that starts within the region τ with specific initial conditions, it gradually converges to P_0 as $t \to +\infty$. Consequently, the prevalence of Ebola virus disease (EVD) steadily decreases from the host population. Therefore, according to La Salle's invariance principles [23], we can determine that P_0 exhibits global asymptotic stability within the domain τ. □

7.2. Global Stability Analysis of Endemic Equilibrium Point

Our objective here is to come up with a Lyapunov function that facilitates achieving global asymptotic stability.

Theorem 5. *If $R_0 > 1$, the equilibrium point P_1 of model (1) shows Global Asymptotic Stability in region τ for values S_1, E_1, I_{u_1}, I_{a_1}, and H_1. Conversely, if $R_0 < 1$, the model becomes unstable.*

Proof. The Lyapunov function $V_1 : \tau \to \mathbb{R}$ [20] is considered for showing the global stability of model (1) at the EE point P_1, defined as:

$$\begin{aligned} V_1 = K_1(S - S_1 \ln S) + K_2(E - E_1 \ln E) + K_3(I_u - I_{u_1} \ln I_u) \\ + K_4(I_a - I_{a_1} \ln I_a) + K_5(H - H_1 \ln H), \end{aligned} \tag{13}$$

where K_1, K_2, K_3, K_4, and K_5 represent positive constants that will be determined later. When investigating the solution of model (1), we compute the rate of change of V_1 over time, giving the following expression:

$$\begin{aligned}\frac{dV_1}{dt} &= K_1(S-S_1)[-(\eta_1+\alpha_1+\sigma_1)E-(\eta_2+\sigma_2)I_u-(\eta_3+\sigma_3)I_a-\mu]\\ &+K_2(E-E_1)[(\eta_1+\alpha_1+\sigma_1)S-\alpha_2 I_u-\alpha_3 I_a-(\mu+\delta_1)]\\ &+K_3(I_u-I_{u_1})[(\eta_2+\sigma_2)S+\alpha_2 E-\alpha_4 H-(\mu+\delta_2+\alpha_6)]\\ &+K_4(I_a-I_{a_1})[(\eta_3+\sigma_3)S+\alpha_3 E-\alpha_5 H-(\mu+\delta_3+\alpha_7)]\\ &+K_5(H-H_1)[\alpha_4 I_u+\alpha_5 I_a-(\mu+\delta_4+\alpha_8)].\end{aligned} \tag{14}$$

As $P_1=(S_1,E_1,I_{u_1},I_{a_1},H_1,R_1)$ represents an EE point, by substituting the LHS of all equations of (1) as follows:

$$\frac{dS_1}{dt}=\frac{dE_1}{dt}=\frac{dI_{u_1}}{dt}=\frac{dI_{a_1}}{dt}=\frac{dH}{dt}=0,$$

which implies that:

$$\begin{cases}\mu=\frac{\Lambda}{S_1}-(\eta_1+\alpha_1+\sigma_1)E_1-(\eta_2+\sigma_2)I_{u_1}-(\eta_3+\sigma_3)I_{a_1},\\ \mu+\delta_1=(\eta_1+\alpha_1+\sigma_1)S_1-\alpha_2 I_{u_1}-\alpha_3 I_{a_1},\\ \mu+\delta_2+\alpha_6=(\eta_2+\sigma_2)S_1+\alpha_2 E_1-\alpha_4 H_1,\\ \mu+\delta_3+\alpha_7=(\eta_3+\sigma_3)S_1+\alpha_3 E_1-\alpha_5 H_1,\\ \mu+\delta_4+\alpha_8=\alpha_4 I_{u_1}+\alpha_5 I_{a_1}.\end{cases} \tag{15}$$

Substituting (15) in (14) and taking $K_1=K_2=K_3=K_4=K_5=1$, we get:

$$\frac{dV_1}{dt}=K_1(S-S_1)(\frac{\Lambda}{S}-\frac{\Lambda}{S_1}).$$

This implies:

$$\frac{dV_1}{dt}=-\Lambda\frac{(S-S_1)^2}{SS_1}\leq 0.$$

Hence, V_1 represents a Lyapunov function. The condition $\frac{dV_1}{dt}=0$ remains valid if $(S,E,I_a,I_u,H,R)=(S_1,E_1,I_{u_1},I_{a_1},H_1,R_1)=P_1$, thus indicating that the point P_1 accounts for the most extensive invariant subset in set:

$$\varepsilon_1=\{(S,E,I_u,I_a,H,R)\in\tau:\frac{dV_1}{dt}=0\}.$$

This means that anywhere a solution trajectory that begins within the feasible region, τ gradually converges to P_1 as $t\to+\infty$. Consequently, the prevalence of EVD steadily increases from the host population. Hence, according to La Salle's invariance principle [23], we can determine that P_1 exhibits global asymptotic stability within the domain τ. □

8. Bifurcation Existence in EVD Epidemic Model

Bifurcation in mathematical models involves small parameter changes causing notable changes in system behavior. It identifies critical points where system dynamics fundamentally change, aiding our understanding of system evolution under varying conditions.

For bifurcation analysis, we will apply central manifold theory, as detailed in [24]. To investigate bifurcation in our model, we set $R_0=1$ to determine b_1^*, where $b_1^*=\eta_1+\alpha_1+\sigma_1$.

$$\begin{aligned} R_0 &= \frac{\Lambda b_1^*}{\mu(\mu+\delta_1)} = 1. \\ \Rightarrow b_1^* &= \frac{\mu(\mu+\delta_1)}{\Lambda} = \frac{\mu b_4}{\Lambda}. \end{aligned}$$

where $b_4 = \mu + \delta_1$, the Jacobian matrix for model (1) at P_0 in DFE proceeds as below:

$$J^{|0|} = \begin{pmatrix} -\mu & -\frac{\Lambda}{\mu}b_1^* & -\frac{\Lambda}{\mu}b_2 & -\frac{\Lambda}{\mu}b_3 & 0 & 0 \\ 0 & \frac{\Lambda}{\mu}b_1^* - b_4 & 0 & 0 & 0 & 0 \\ 0 & 0 & \frac{\Lambda}{\mu}b_2 - b_5 & 0 & 0 & 0 \\ 0 & 0 & 0 & \frac{\Lambda}{\mu}b_3 - b_6 & 0 & 0 \\ 0 & 0 & 0 & 0 & -b_7 & 0 \\ 0 & 0 & \alpha_6 & \alpha_7 & \alpha_8 & -\mu \end{pmatrix}.$$

Let us define the following parameters:

$b_1 = (\eta_1 + \alpha_1 + \sigma_1)$, $b_2 = (\eta_2 + \sigma_2)$, $b_3 = (\eta_3 + \sigma_3)$, $b_4 = (\mu + \delta_1)$, $b_5 = (\mu + \delta_2 + \alpha_6)$, $b_6 = (\mu + \delta_3 + \alpha_7)$, $b_7 = (\mu + \delta_4 + \alpha_8)$.

Upon calculation, the Jacobian matrix $J^{|0|}$ eigenvalues are given as follows:

$$\begin{aligned} \lambda_{1,2} &= -\mu, \\ \lambda_3 &= -(\mu + \delta_4 + \alpha_8), \\ \lambda_4 &= \frac{\Lambda}{\mu}(\eta_3 + \sigma_3) - (\mu + \delta_3 + \alpha_7), \\ \lambda_5 &= \frac{\Lambda}{\mu}(\eta_2 + \sigma_2) - (\mu + \delta_2 + \alpha_6), \\ \lambda_6 &= (\mu + \delta_1)(R_0 - 1). \end{aligned}$$

For $R_0 = 1$, $\lambda_6 = 0$. Thus, we have one zero eigenvalue, indicating that a bifurcation exists.

Identifying the Nature of Bifurcation

This subsection analyzes the nature of the bifurcation presented in our model. To do so, the process involves identifying both the left and right eigenvectors, and then, based on these eigenvectors, ascertaining the type of bifurcation present, as outlined in [24].

$$J^{|0|}(b_1^*).U = 0.$$

$$\begin{pmatrix} -\mu & -\frac{\Lambda}{\mu}b_1^* & -\frac{\Lambda}{\mu}b_2 & -\frac{\Lambda}{\mu}b_3 & 0 & 0 \\ 0 & \frac{\Lambda}{\mu}b_1^* - b_4 & 0 & 0 & 0 & 0 \\ 0 & 0 & \frac{\Lambda}{\mu}b_2 - b_5 & 0 & 0 & 0 \\ 0 & 0 & 0 & \frac{\Lambda}{\mu}b_3 - b_6 & 0 & 0 \\ 0 & 0 & 0 & 0 & -b_7 & 0 \\ 0 & 0 & \alpha_6 & \alpha_7 & \alpha_8 & -\mu \end{pmatrix} \begin{pmatrix} u_1 \\ u_2 \\ u_3 \\ u_4 \\ u_5 \\ u_6 \end{pmatrix} = \begin{pmatrix} 0 \\ 0 \\ 0 \\ 0 \\ 0 \\ 0 \end{pmatrix},$$

which gives:

$$\begin{pmatrix} -\mu u_1 - \frac{\Lambda}{\mu} b_1^* u_2 - \frac{\Lambda}{\mu} b_2 u_3 - \frac{\Lambda}{\mu} b_3 u_4 \\ \left(\frac{\Lambda}{\mu} b_1^* - b_4\right) u_2 \\ \left(\frac{\Lambda}{\mu} b_2 - b_5\right) u_3 \\ \left(\frac{\Lambda}{\mu} b_3 - b_6\right) u_4 \\ -b_7 u_5 \\ \alpha_6 u_3 + \alpha_7 u_4 + \alpha_8 u_5 - \mu u_6 \end{pmatrix} = \begin{pmatrix} 0 \\ 0 \\ 0 \\ 0 \\ 0 \\ 0 \end{pmatrix}.$$

Therefore:

$$-\mu u_1 - \frac{\Lambda}{\mu} b_1^* u_2 - \frac{\Lambda}{\mu} b_2 u_3 - \frac{\Lambda}{\mu} b_3 u_4 = 0, \tag{16}$$

$$\left(\frac{\Lambda}{\mu} b_1^* - b_4\right) u_2 = 0, \tag{17}$$

$$\left(\frac{\Lambda}{\mu} b_2 - b_5\right) u_3 = 0, \tag{18}$$

$$\left(\frac{\Lambda}{\mu} b_3 - b_6\right) u_4 = 0, \tag{19}$$

$$-b_7 u_5 = 0, \tag{20}$$

$$\alpha_6 u_3 + \alpha_7 u_4 + \alpha_8 u_5 - \mu u_6 = 0. \tag{21}$$

After solving Equations (16)–(21), we have $u_1 = 0$, $u_2 = 0$, $u_3 = 0$, $u_4 = 0$, $u_5 = 0$, and $u_6 = 0$. Therefore, the right eigenvector is zero.

For the zero eigenvalues, the left eigenvector is as follows:

$$C.J^{|0|}(b_1^*) = 0.$$

$$\begin{pmatrix} c_1 & c_2 & c_3 & c_4 & c_5 & c_6 \end{pmatrix} \begin{pmatrix} -\mu & -\frac{\Lambda}{\mu} b_1^* & -\frac{\Lambda}{\mu} b_2 & -\frac{\Lambda}{\mu} b_3 & 0 & 0 \\ 0 & \frac{\Lambda}{\mu} b_1^* - b_4 & 0 & 0 & 0 & 0 \\ 0 & 0 & \frac{\Lambda}{\mu} b_2 - b_5 & 0 & 0 & 0 \\ 0 & 0 & 0 & \frac{\Lambda}{\mu} b_3 - b_6 & 0 & 0 \\ 0 & 0 & 0 & 0 & -b_7 & 0 \\ 0 & 0 & \alpha_6 & \alpha_7 & \alpha_8 & -\mu \end{pmatrix} = Q,$$

where

$$Q = \begin{pmatrix} 0 & 0 & 0 & 0 & 0 & 0 \end{pmatrix}.$$

After multiplying these matrices and equating them to zero, we obtain:

$$-\mu c_1 = 0, \tag{22}$$

$$-\frac{\Lambda}{\mu} b_1^* c_1 + \left(\frac{\Lambda}{\mu} b_1^* - b_4\right) c_2 = 0, \tag{23}$$

$$-\frac{\Lambda}{\mu} b_2 c_1 + \left(\frac{\Lambda}{\mu} b_2 - b_5\right) c_3 + \alpha_6 c_6 = 0, \tag{24}$$

$$-\frac{\Lambda}{\mu} b_3 c_1 + \left(\frac{\Lambda}{\mu} b_3 - b_6\right) c_4 + \alpha_7 c_6 = 0, \tag{25}$$

$$-b_7 c_5 + \alpha_8 c_6 = 0, \tag{26}$$

$$-\mu v_6 = 0. \tag{27}$$

When we solve Equations (22)–(27), we have $c_1 = 0$, $c_2 = 0$, $c_3 = 0$, $c_4 = 0$, $c_5 = 0$, and $c_6 = 0$. Thus, the left eigenvector also equals zero. As both the right and left eigenvectors are zero, this represents a trivial case.

9. Sensitivity Analysis of R_0

In this study, conducting a sensitivity analysis on model parameters regarding R_0 is crucial for identifying key factors influencing disease transmission and control. We evaluate parameter significance relative to R_0 using the formula by Chitnis et al. [25]. The definition of the sensitivity index on R_0 is

$$\Upsilon_{\kappa}^{R_0} = \frac{\partial R_0}{\partial \kappa} \times \frac{\kappa}{R_0}, \quad \kappa \in \{\Lambda,\ \mu,\ \delta_1,\ \eta_1,\ \alpha_1,\ \sigma_1\}.$$

$$\begin{aligned}
\Upsilon_{\Lambda}^{R_0} &= \frac{\partial}{\partial \Lambda}\left(\frac{\Lambda(\eta_1+\alpha_1+\sigma_1)}{\mu(\mu+\delta_1)}\right) \times \frac{\Lambda\mu(\mu+\delta_1)}{\Lambda(\eta_1+\alpha_1+\sigma_1)} = 1,\\
\Upsilon_{\mu}^{R_0} &= \frac{\partial}{\partial \mu}\left(\frac{\Lambda(\eta_1+\alpha_1+\sigma_1)}{\mu(\mu+\delta_1)}\right) \times \frac{\mu^2(\mu+\delta_1)}{\Lambda(\eta_1+\alpha_1+\sigma_1)} = -1 - \frac{\mu}{\mu+\delta_1} = -1.7854\\
\Upsilon_{\delta_1}^{R_0} &= \frac{\partial}{\partial \delta_1}\left(\frac{\Lambda(\eta_1+\alpha_1+\sigma_1)}{\mu(\mu+\delta_1)}\right) \times \frac{\delta_1\mu(\mu+\delta_1)}{\Lambda(\eta_1+\alpha_1+\sigma_1)} = -\frac{\delta_1}{\mu+\delta_1} = -0.2145,\\
\Upsilon_{\eta_1}^{R_0} &= \frac{\partial}{\partial \eta_1}\left(\frac{\Lambda(\eta_1+\alpha_1+\sigma_1)}{\mu(\mu+\delta_1)}\right) \times \frac{\eta_1\mu(\mu+\delta_1)}{\Lambda(\eta_1+\alpha_1+\sigma_1)} = \frac{\eta_1}{\eta_1+\alpha_1+\sigma_1} = 0.1521,\\
\Upsilon_{\alpha_1}^{R_0} &= \frac{\partial}{\partial \alpha_1}\left(\frac{\Lambda(\eta_1+\alpha_1+\sigma_1)}{\mu(\mu+\delta_1)}\right) \times \frac{\alpha_1\mu(\mu+\delta_1)}{\Lambda(\eta_1+\alpha_1+\sigma_1)} = \frac{\alpha_1}{\eta_1+\alpha_1+\sigma_1} = 0.3547,\\
\Upsilon_{\sigma_1}^{R_0} &= \frac{\partial}{\partial \sigma_1}\left(\frac{\Lambda(\eta_1+\alpha_1+\sigma_1)}{\mu(\mu+\delta_1)}\right) \times \frac{\sigma_1\mu(\mu+\delta_1)}{\Lambda(\eta_1+\alpha_1+\sigma_1)} = \frac{\sigma_1}{\eta_1+\alpha_1+\sigma_1} = 0.4931.
\end{aligned}$$

The sensitivity analysis of R_0 concerning the model parameters is illustrated in Figure 3. Sensitivity analysis of R_0 concerning all parameters encompasses both numerical computation and graphical representation. In these parameters, Λ, η_1, α_1, and σ_1 exert a positive influence on R_0, whereas μ and δ_1 exhibit a negative impact. Therefore, one can conclude that the most sensitive parameters are Λ and μ.

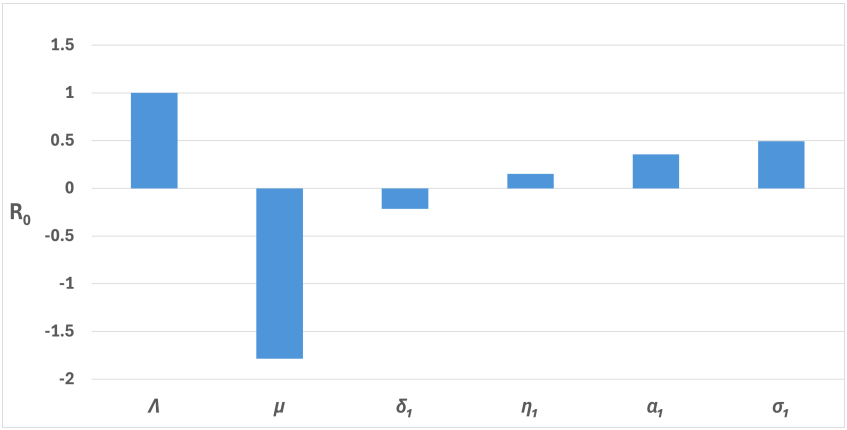


Figure 3. Sensitivity index of R_0 for the model parameters.

10. Numerical Simulations

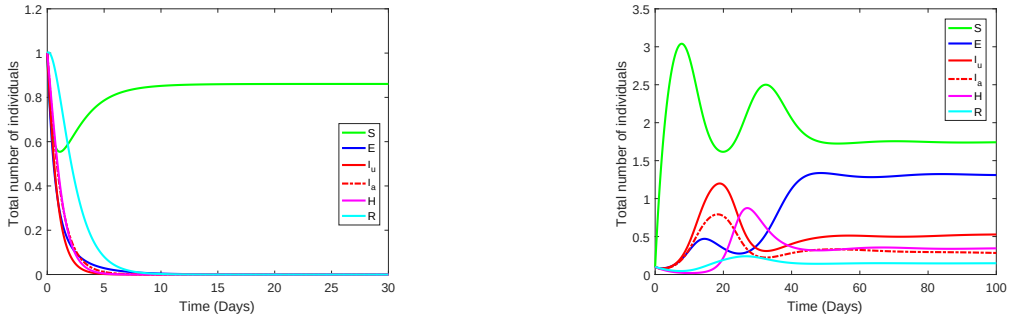
This section focuses on the numerical simulations of the proposed model. To better understand how the model system (1) behaves dynamically in different scenarios, we conducted numerical simulations using the RK4 method and MATLAB R2023b. These simulations used the parameter values listed in Table 2. In addition to time-series plots, we focused on revealing key dynamical behaviors such as bifurcation curves, limit cycles,

and other relevant dynamical structures to provide a comprehensive understanding of the model's dynamics. Appropriate parameter ranges were selected to visualize these phenomena.

Table 2. Assigned values to the parameters of system (1) for simulation purposes.

Parameter	Value	Source	Parameter	Value	Source
Λ	0.63210	[14]	μ	0.43740	Assumed
δ_1	0.20060	[14]	δ_2	0.00210	[26]
δ_3	0.00130	Assumed	δ_4	0.00120	Assumed
α_1	0.28770	[14]	α_2	0.10000	[26]
α_3	0.00190	[26]	α_4	0.00100	[26]
α_5	0.00050	[26]	α_6	0.00210	[26]
α_7	0.00140	Assumed	α_8	0.00010	[26]
η_1	0.12340	[14]	η_2	0.24310	[14]
η_3	0.08100	Assumed	σ_1	0.40000	[14]
σ_2	0.30000	[14]	σ_3	0.10000	Assumed

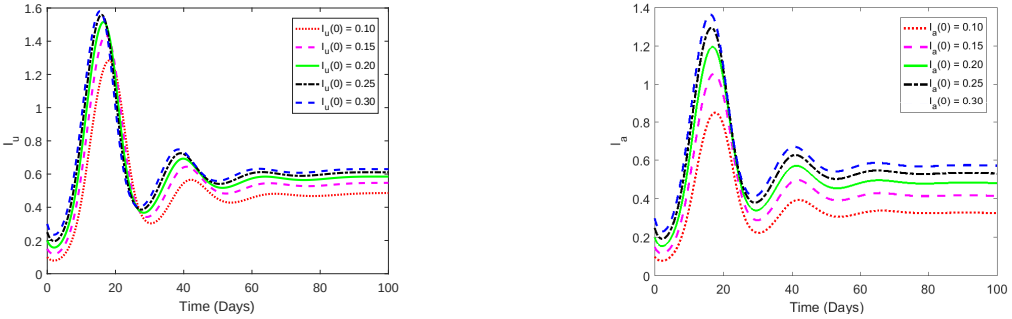
Figure 4 illustrates the variation in the total number of individuals over time for different values of R_0, demonstrating both the disease-free equilibrium (DFE) and endemic equilibrium (EE).



(**a**) (**b**)

Figure 4. Variation of the total number of individuals over time for: (**a**) $\eta_1 = 0.01234$, $\alpha_1 = 0.02877$, $\sigma_1 = 0.04000$, and $R_0 = 0.1837$ (<1); (**b**) $\eta_1 = 0.1234$, $\alpha_1 = 2877$, $\sigma_1 = 0.4000$, and $R_0 = 1.8372$ (>1).

To explore the emergence of limit cycles and periodic behaviors, we conducted further simulations for parameter values leading to oscillatory dynamics. In Figure 5, we examine the variation in the total number of infectious individuals over time for different initial conditions when $R_0 > 1$, highlighting the stability of endemic equilibrium. This figure shows how the total number of infected individuals changes over time, even under different initial conditions.



(**a**) Infectious individuals with different initial conditions for I_u (untreated infections).

(**b**) Infectious individuals with different initial conditions for I_a (AIDS cases).

Figure 5. Variation of the total number of infectious individuals over time with different initial values for $R_0 > 1$. Subfigure (**a**) shows the variation for I_u, representing untreated infections, while subfigure (**b**) illustrates the variation for I_a, representing AIDS cases.

Finally, in Figure 6, we present bifurcation diagrams that depict the system's transitions as parameters such as α_1, η_1, and σ_1 vary. These diagrams reveal the existence of limit cycles and bifurcation points, providing deeper insights into the dynamics of the infected population.

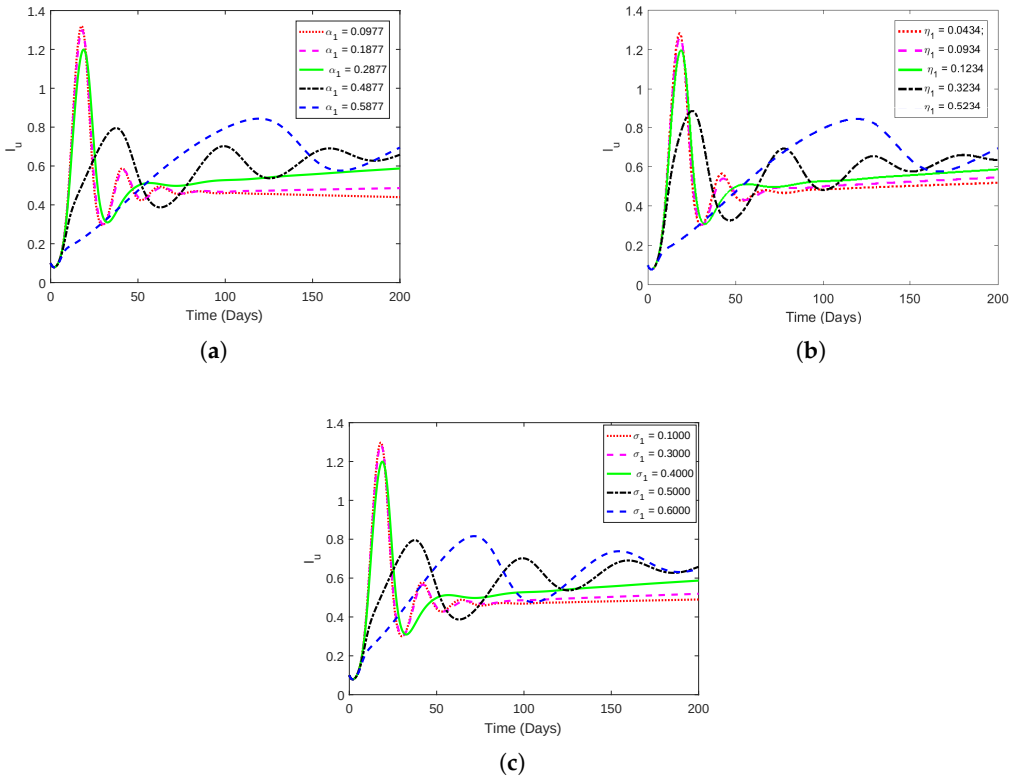


Figure 6. Effects of Parameters α_1, η_1, and σ_1 on the Infected Population (I_u). (**a**) Effects of α_1 on I_u. (**b**) Effects of η_1 on I_u. (**c**) Effects of σ_1 on I_u.

If $\eta_1 = 0.01234$, $\alpha_1 = 0.02877$, and $\sigma_1 = 0.04000$, then $R_0 = 0.1837$ (which is less than 1). As a result, the number of susceptible individuals over time initially rises, reaching a peak before leveling off into a steady trend (DFE). On the other hand, the numbers of exposed, unaware infected, aware infected, hospitalized, and recovered individuals all show a declining trend over time, as shown in Figure 4a. If $\eta_1 = 0.1234$, $\alpha_1 = 0.2877$, and $\sigma_1 = 0.4000$, yields $R_0 = 1.8372$ (which is greater than 1). As a result, the system reaches a state of equilibrium known as endemic equilibrium, shown in Figure 4b. The analysis also explores how parameter variation influences the emergence of limit cycles and complex dynamics. Figure 5a,b show how the fraction of the total number of infected individuals changes over time when R_0 is greater than 1. These figures illustrate that for a specific value of R_0, the behavior of the number of infected individuals remains consistent, even with different initial numbers of infected individuals. Additionally, the impact of parameters α_1, η_1, and σ_1 on the infected population (I_u) is also depicted in Figure 6, demonstrating how bifurcation curves and limit cycles arise under varying parameter ranges.

11. Conclusions

To summarize, our research provides a novel and enhanced approach to modeling Ebola virus disease (EVD), improving our understanding of disease transmission dynamics and effective countermeasures. The mathematical model introduced in this study incorporates both aware and unaware infected individuals, as well as hospitalized patients, offering a more detailed representation of EVD dynamics. The key findings show that for $R_0 < 1$, the disease-free equilibrium is stable, meaning the disease will die out, while for $R_0 > 1$, the endemic equilibrium is stable, indicating that the disease will persist. Sensitivity

analysis revealed that the transmission and recovery rates are the most influential factors in controlling R_0.

These results have significant implications for public health policy and resource allocation, as they suggest that increasing public awareness and enhancing hospital capacities are critical strategies in managing outbreaks. Additionally, our model's bifurcation analysis underscores the potential for abrupt changes in disease dynamics based on small parameter variations, further informing intervention strategies. Through numerical simulations, we have demonstrated the practical application of our model, which can guide the optimization of healthcare resources and the development of policies to mitigate the spread of Ebola and similar infectious diseases.

Author Contributions: Conceptualization, I.U. and I.A.; methodology, I.U.; software, I.U.; validation, I.A., N.A. and I.U.H.; formal analysis, I.A.; investigation, I.U.; resources, N.A.; data curation, M.I.; writing—original draft preparation, I.U.H.; writing—review and editing, I.A. and M.Y.; visualization, M.I.; supervision, M.D.A.; project administration, I.A. and M.Y. All authors have read and agreed to the published version of the manuscript.

Funding: No specific money, whether from the public, commercial, or nonprofit sectors, was given to this research.

Data Availability Statement: All information is accessible.

Conflicts of Interest: The authors declare no conflict of interest.

References

1. Leroy, E.M.; Kumulungui, B.; Pourrut, X. Fruit bats as reservoirs of Ebola virus. *Nature* **2015**, *438*, 575–576. [CrossRef] [PubMed]
2. Tahir, M.; Shah, S.I.A.; Zaman, G.; Muhammad, S. Ebola virus epidemic disease its modelling and stability analysis required abstain strategies. *Cogent Biol.* **2018**, *4*, 1488511. [CrossRef]
3. Ahmad, W.; Rafiq, M.; Abbas, M. Mathematical analysis to control the spread of Ebola virus epidemic through voluntary vaccination. *Eur. Phys. J. Plus* **2020**, *135*, 775. [CrossRef]
4. Yazdani, N.; Abbas, A. Pakistan adopts defensive strategies against Ebola contagion. *Arch. Pharm. Pract.* **2015**, *6*, 13–15. [CrossRef]
5. Zhou, L.; Fan, M. Dynamics of an SIR model with limited medical resources revisited. *Nonlinear Anal. Real World Appl.* **2012**, *13*, 312–324. [CrossRef]
6. Nouvellet, P.; Garske, T.; Mills, H.L.; Gilani, G.N.; Hinsley, W.; Blake, I.M.; Ferguson, N.M. The role of rapid diagnostics in managing Ebola epidemics. *Nature* **2015**, *528*, 109–116. [CrossRef]
7. Lewnard, J.A.; Mbah, M.L.N.; Murillo, J.A.; Altice, F.L.; Bawo, L.; Nyenswah, T.G.; Galvani, A.P. Dynamics and control of Ebola virus transmission in Montserrado, Liberia: A mathematical modelling analysis. *Lancet Infect. Dis.* **2014**, *14*, 1189–1195. [CrossRef]
8. Fatima, B.; Yavuz, M.; ur Rahman, M.; Althobaiti, A.; Althobaiti, S. Predictive Modeling and Control Strategies for the Transmission of Middle East Respiratory Syndrome Coronavirus. *Math. Comput. Appl.* **2023**, *28*, 98. [CrossRef]
9. Kamrujjaman, M.; Sinje, S.S.; Nandi, T.R.; Islam, F.; Rahman, M.A.; Akhi, A.A.; Alam, M.S. The impact of the COVID-19 pandemic on education in Bangladesh and its mitigation. *Bull. Biomath.* **2024**, *2*, 57–84. [CrossRef]
10. Rachah, A.; Torres, D.F.M. Mathematical modelling, simulation, and optimal control of the 2014 Ebola outbreak in West Africa. *Discret. Dyn. Nat. Soc.* **2015**, *2015*, 842792. [CrossRef]
11. Njankou, S.D.; Nyabadza, F. An optimal control model for Ebola virus disease. *J. Biol. Syst.* **2016**, *24*, 29–49. [CrossRef]
12. Haq, I.U.; Yavuz, M.; Ali, N.; Akgül, A. A SARS-CoV-2 Fractional-Order Mathematical Model via the Modified Euler Method. *Math. Comput. Appl.* **2022**, *27*, 82. [CrossRef]
13. Yavuz, M.; Akyüz, K.; Bayraktar, N.B.; Ozdemir, F.N. Hepatitis-B disease modelling of fractional order and parameter calibration using real data from the USA. *AIMS Biophy.* **2024**, *11*, 378–402. [CrossRef]
14. Rafiq, M.; Ahmad, W.; Abbas, M.; Baleanu, D. A reliable and competitive mathematical analysis of Ebola epidemic model. *Adv. Differ. Equ.* **2020**, *2020*, 540. [CrossRef]
15. Joshi, H.; Yavuz, M.; Özdemir, N. Analysis of novel fractional order plastic waste model and its effects on air pollution with treatment mechanism. *J. Appl. Anal. Comput.* **2024**, *14*, 3078–3098.
16. Adu, I.K.; Wireko, F.A.; Adarkwa, S.A.; Agyekum, G.O. Mathematical analysis of Ebola considering transmission at treatment centres and survivor relapse using fractal-fractional Caputo derivatives in Uganda. *Math. Model. Numer. Simul. Appl.* **2024**, *4*, 296–334. [CrossRef]
17. Berge, T.; Bowong, S.; Lubuma, J.M.S.; Manyombe, M.L.M. Modeling Ebola Virus Disease Transmissions with Reservoir in a Complex Virus Life Ecology. *Math. Biosci. Eng.* **2018**, *15*, 21–56. [CrossRef]
18. Ali, N.; Zaman, G.; Chohan, M.I. Global stability of a delayed HIV-1 model with saturations response. *Appl. Math. Inf. Sci.* **2017**, *11*, 189–194. [CrossRef]

19. Tang, Y.; Yuan, R.; Ma, Y. Dynamical behaviors determined by the Lyapunov function in competitive Lotka-Volterra systems. *Phys. Rev. E* **2013**, *87*, 012708. [CrossRef]
20. Berge, T.; Lubuma, J.S.; Moremedi, G.M.; Morris, N.; Kondera-Shava, R. A simple mathematical model for Ebola in Africa. *J. Biol. Dyn.* **2017**, *11*, 42–74. [CrossRef]
21. Espinoza, B.; Moreno, V.; Bichara, D.; Chavez, C.C. Assessing the Efficiency of Cordon Sanitaire as a Control Strategy of Ebola. *arXiv* **2015**, arXiv:1510.07415.
22. Fasina, F.O.; Shittu, A.; Lazarus, D.; Tomori, O.; Simonsen, L.; Viboud, C.; Chowell, G. Transmission dynamics and control of Ebola virus disease outbreak in Nigeria, July to September 2014. *Eurosurveillance* **2014**, *19*, 20920. [CrossRef] [PubMed]
23. Routh, E. *Advanced Dynamics of a System of Rigid Bodies*; MacMillan: London, UK, 1905.
24. Vanderbauwhede, A.; Iooss, G. *Center Manifold Theory in Infinite Dimensions*; Springer: Berlin/Heidelberg, Germany, 1992; pp. 125–163.
25. Rakkiyappan, R.; Balasubramaniam, P. Delay-dependent asymptotic stability for stochastic delayed recurrent neural networks with time varying delays. *Appl. Math. Comput.* **2008**, *198*, 526–533. [CrossRef]
26. Edward, S.; Lusekelo, E.M.; Ndidi, D.M.; Simanjilo, E. Mathematical modelling of the transmission dynamics of Ebola virus disease with control strategies. *Int. J. Sci. Basic Appl. Res.* **2017**, *33*, 112–130.

Disclaimer/Publisher's Note: The statements, opinions and data contained in all publications are solely those of the individual author(s) and contributor(s) and not of MDPI and/or the editor(s). MDPI and/or the editor(s) disclaim responsibility for any injury to people or property resulting from any ideas, methods, instructions or products referred to in the content.